

Parametric Study of a Microwave Absorber Based on Metamaterials.

Department of Electrical & Computer Engineering

University of Western Macedonia

Markos Delaportas *

March 2025

Abstract – Microwave absorbers play a crucial role in modern telecommunications and electronic systems by mitigating unwanted electromagnetic interference (EMI) and enhancing the performance of various devices. These absorbers are essential in applications ranging from radar systems and anechoic chambers to consumer electronics and medical devices. Traditional microwave absorbers, while effective, often suffer from limitations such as bulkiness and narrow bandwidth. Metamaterial-based microwave absorbers offer a promising alternative due to their unique electromagnetic properties, which are not found in natural materials. These engineered materials can achieve near-unity absorption across a wide range of frequencies, making them highly efficient. The advantages of metamaterial absorbers include their thin profile, lightweight nature, and the ability to tailor their absorption characteristics through precise structural design. This makes them ideal for applications requiring compact and efficient EMI mitigation. Additionally, metamaterial absorbers can be designed to operate over multiple frequency bands, providing versatility and enhanced performance in complex electromagnetic environments.

Contents

I Introduction	1
II Theoretical Study	2
III Simulation	3
III.I CST Implementation	3
III.II Evaluation	6
III.III Alternative Modeling Methods	7
IV Optimization	10
IV.I CST Optimizer	10
V Discussion	13

I Introduction

Metamaterials are artificially designed materials that exhibit peculiar properties like negative refractive index [1], Snell's law reversal [2], Doppler effect reverse [3], and left-handed behavior. These properties make them suitable for various applications,

*E-mail: ece01316@uowm.gr

including perfect absorption. Metamaterial absorbers can achieve near-unity absorption, thin profiles, lightweight characteristics, and design flexibility.

The development of metamaterial absorbers has seen significant progress, with researchers exploring various designs and materials to enhance their performance. Metamaterial absorbers are predominantly used in the microwave, terahertz, and optical frequency spectra. Recent advancements include the development of multi-band polarization-insensitive metamaterial absorbers for microwave applications, broadband microwave coding metamaterial absorbers [4], and ultra-wideband origami microwave absorbers[5].

This study begins with a theoretical exploration of absorber devices and the unique properties of metamaterials that make them suitable for electromagnetic wave absorption. Following this, the report details the implementation of a specific microwave absorber device using advanced simulation software, highlighting the practical aspects of device design and performance evaluation. Finally, the report addresses the parametric design and optimization of the device, fine-tuning structural parameters to achieve optimal absorption characteristics. Through this comprehensive approach, the report aims to provide a thorough understanding of the principles, design methodologies, and practical applications of metamaterial-based microwave absorbers.

II Theoretical Study

Metamaterials are artificially engineered materials with unique electromagnetic properties not found in nature. They are designed with specific geometrical structures that allow them to exhibit properties like negative refractive index, reverse Snell's law, and right/left-handed behavior. The first to coin the term of metamaterial absorbers was Victor Veselago [1].

An MMA typically comprises three layers:

- A periodic metallic pattern on top
- A dielectric substrate in the middle
- A bottom metallic ground plane

As multi-layer structures in MMAs enable broadband absorption by creating multiple resonant frequencies. By stacking different layers with varying properties, a wider range of frequencies can be absorbed effectively.

Impedance matching is crucial for MMAs to minimize reflection and maximize absorption. This is achieved when the impedance of the MMA is matched to the impedance of free space, ensuring that incident electromagnetic waves are absorbed rather than reflected.

In order to evaluate the absorption of the microwave metamaterial absorber proposed in this study [6] the reflection and transmission power shall be calculated as well as the reflection coefficient. The bare necessary equations are shown in (1).

$$Z = Z_0 \sqrt{\frac{\mu_r}{\epsilon_r}} \quad (1a)$$

$$\Gamma = \frac{Z - Z_0}{Z + Z_0} \quad (1b)$$

$$T = \frac{2Z_0}{Z + Z_0} \quad (1c)$$

$$A = 1 - |\Gamma|^2 - |T|^2 \quad (1d)$$

Simulation tools play a crucial role in the design and analysis of metamaterial absorbers. CST Studio Suite is a software package used for high-frequency simulation. It offers various solvers, including time-domain and frequency-domain solvers, for simulating

electromagnetic phenomena [3].

III Simulation

The simulation was conducted using CST (Computer Simulation Technology) software to implement a configuration inspired by the design presented in [6]. This section outlines the steps taken to model the structure, the assumptions made, and the results obtained from the simulation.

III.I CST Implementation

The vertical layout in CST consists of a three-layer structure:

- **Dielectric Substrate:** This layer serves as the base for the structure.
- **Air Gap:** Positioned above the dielectric substrate, this layer introduces an air gap to influence the electromagnetic properties.
- **Metal Backplate:** The top layer, made of copper, acts as a reflective surface.

The dielectric substrate also includes a metallic component, which is made of the same material as the metal backplate—copper, with a conductivity of $(5.96 \mu 10^7 \text{ S/m})$.

Initially, the FR-4 substrate is placed without the metal resonance layer. The other two layers are positioned below $Z = 0$. When viewed from the orthographic side, the layout appears as shown in Figure (1).

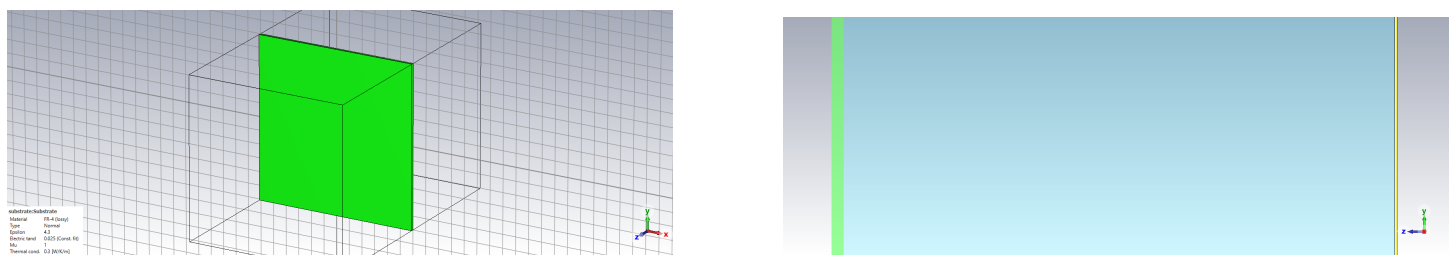


Figure 1: Basic Vertical Layout

Next, a ring resonator is added on top of the dielectric substrate. The ring is made of the same material and thickness as the backplate, as illustrated in Figure (2).

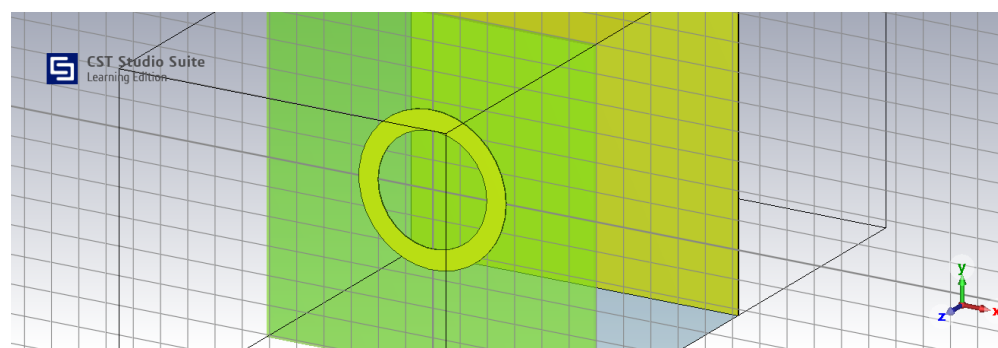


Figure 2: Ring Resonator

An important assumption in this design is that both the body and the tip of the arrow have a width of $\alpha = 0.5\text{mm}$. To accurately place the curve points defining the arrow, a system of equations must be solved to determine the Cartesian coordinates of the arrow's base points. These points lie on the arc of the ring and are equidistant from the curve $y = x$. The following MATLAB code snippet demonstrates the solution to this system:

```

1 syms x1 x2
2
3 eq1 = 2*(x1 - x2)^2 == .5^2; eq2 = sqrt(x2^2 + x1^2) == 2.7;
4
5 sol = solve([eq1, eq2], [x1 x2]); disp([sol.x1 sol.x2]);

```

Listing 1: extraction of arrow base points

This system simplifies to the equations shown in Equation (2).

$$\begin{pmatrix} \sigma_3 - \frac{2916\sigma_1}{1433} & -\sigma_1 \\ \sigma_4 - \frac{2916\sigma_2}{1433} & -\sigma_2 \\ \frac{2916\sigma_1}{1433} - \sigma_3 & \sigma_1 \\ \frac{2916\sigma_2}{1433} - \sigma_4 & \sigma_2 \end{pmatrix}$$

where

$$\sigma_1 = \sqrt{\frac{729}{200} - \frac{7\sqrt{59}}{80}} \quad (2)$$

$$\sigma_2 = \sqrt{\frac{7\sqrt{59}}{80} + \frac{729}{200}}$$

$$\sigma_3 = \frac{400 \left(\frac{729}{200} - \frac{7\sqrt{59}}{80} \right)^{3/2}}{1433}$$

$$\sigma_4 = \frac{400 \left(\frac{7\sqrt{59}}{80} + \frac{729}{200} \right)^{3/2}}{1433}$$

The arrow is then mirrored across the X, Y, and XY planes to cover all four sides of the cell. The face is covered with copper, and a height of $d = 0.035mm$ is assigned, as shown in Figure (3). This step is crucial because all other layers were initially positioned below $Z = 0$.

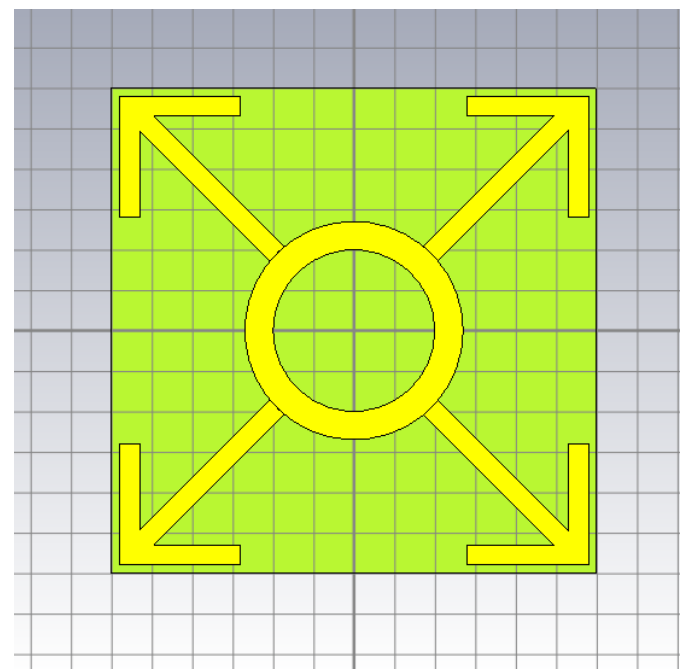
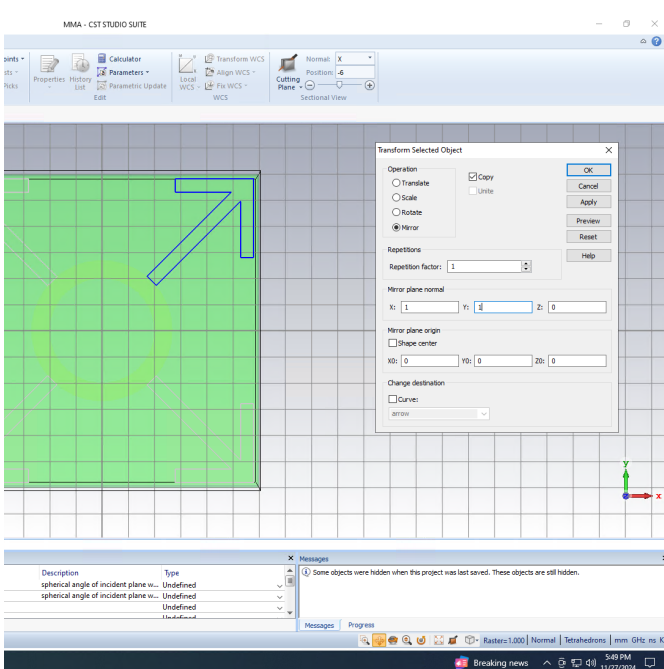


Figure 3: Mirroring Arrow and Cover

A series of cuts (boolean subtractions) are made in the resonance layer to add resistors between the copper faces near the arrows, as depicted in Figure (4).

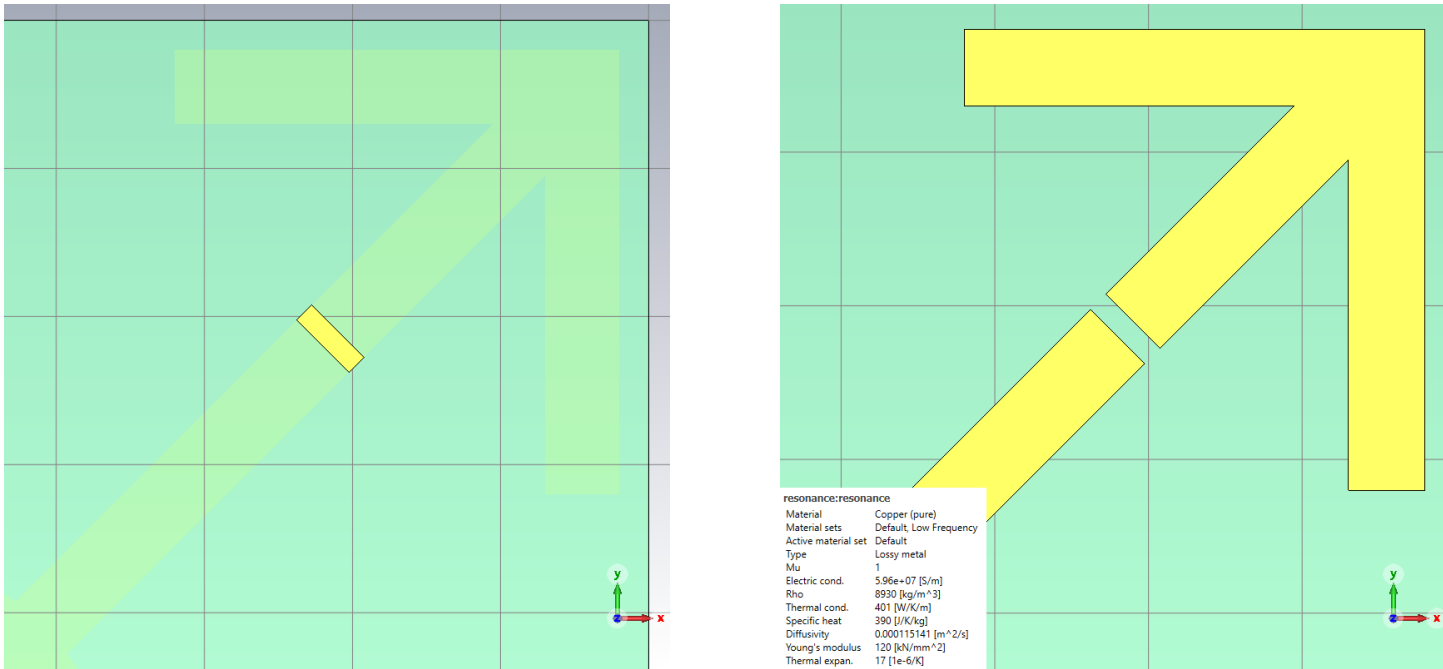


Figure 4: Cuts Near the Arrows

Similar cuts are made near the ring to ensure uniform width, as shown in Figure (5).

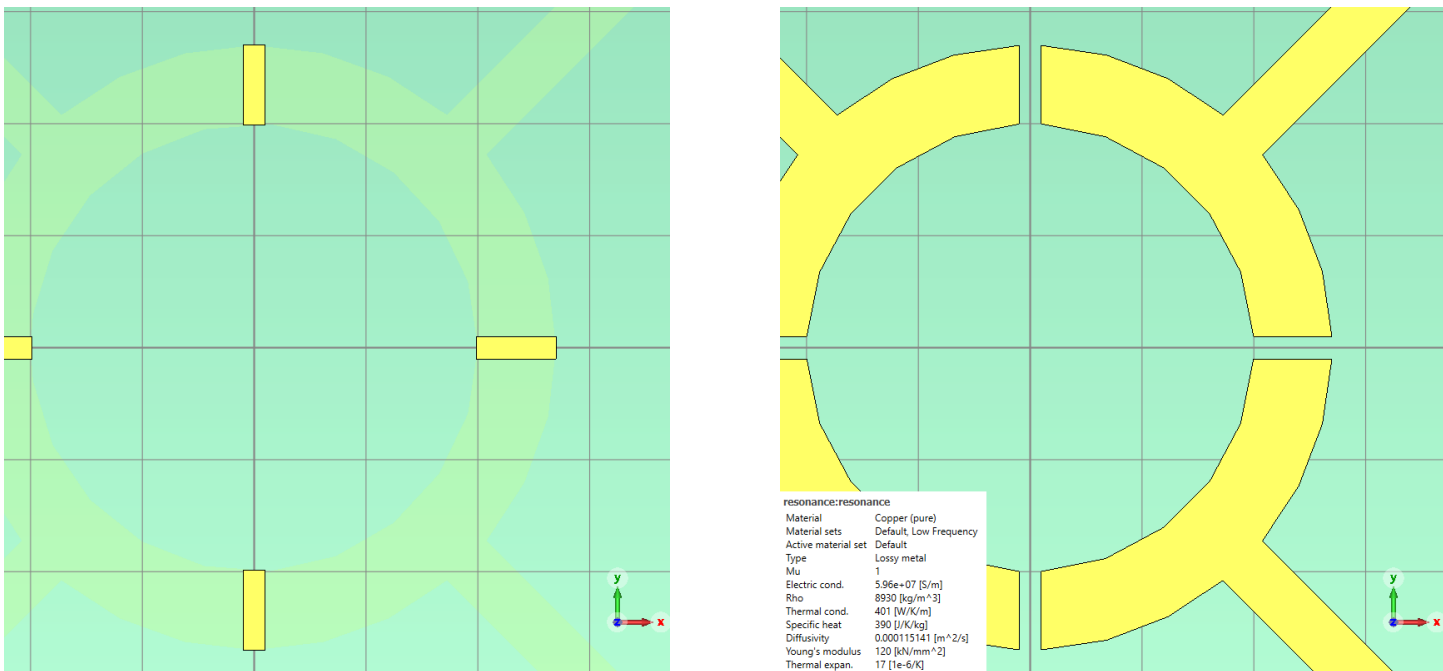


Figure 5: Cuts Near the Ring

Resistors are then added, connecting to the center points of the faces created by the previous subtractions, as illustrated in Figure (6a). It is important to note that the performance of the absorber may be reduced in this implementation. Better absorbance might be achieved if the connection height is set to $d = 0.035\text{mm}$.

To perform the simulation using the frequency solver in CST, periodic boundaries are set along the XY plane, and free space conditions are applied along the Z axis. The resulting mesh is shown in Figure (6b).

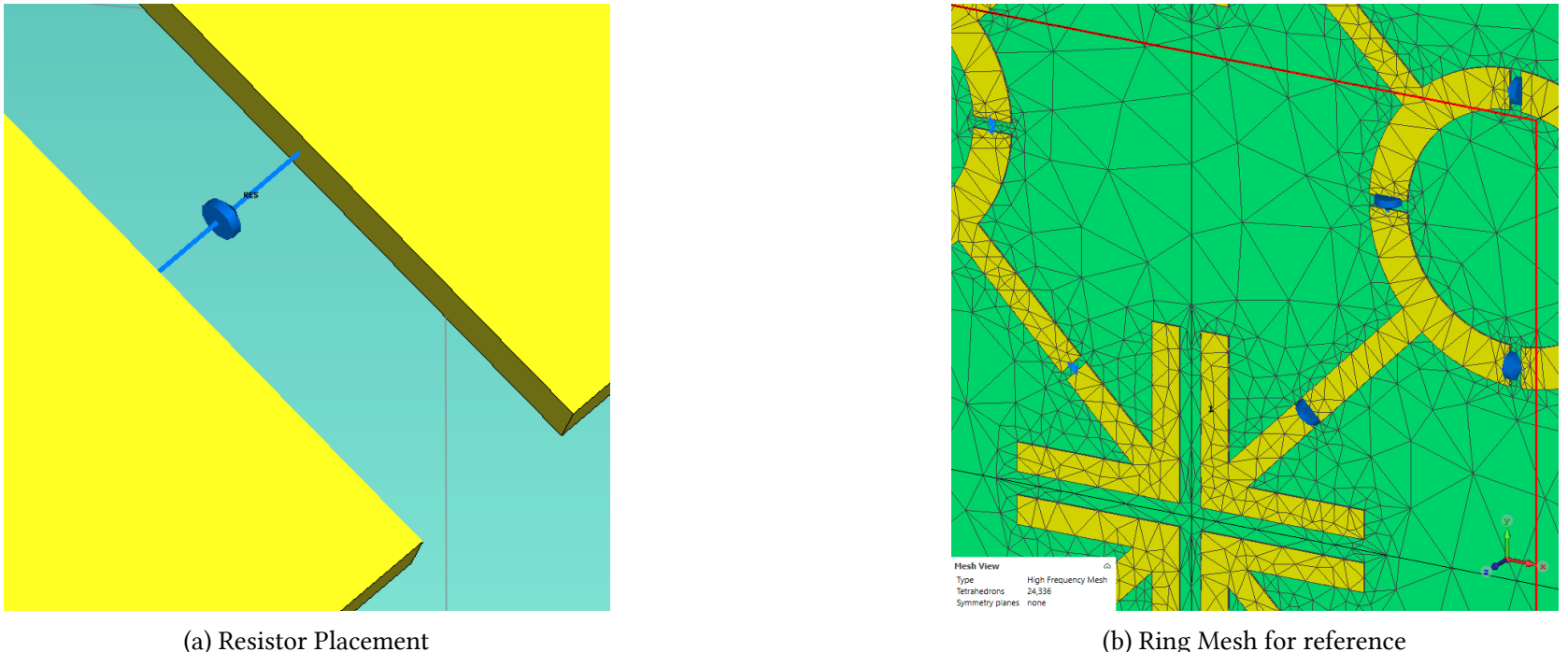


Figure 6: Mesh around Resistors

III.II Evaluation

The electrical field absorbance is analyzed at different frequencies. The first line of figure (7) shows the electrical field for $Z_{max}(1)$ at frequencies of 2.7 GHz, 7.7 GHz, and 12.7 GHz. Similarly the second line of figure (7) shows the electrical field for $Z_{max}(2)$.

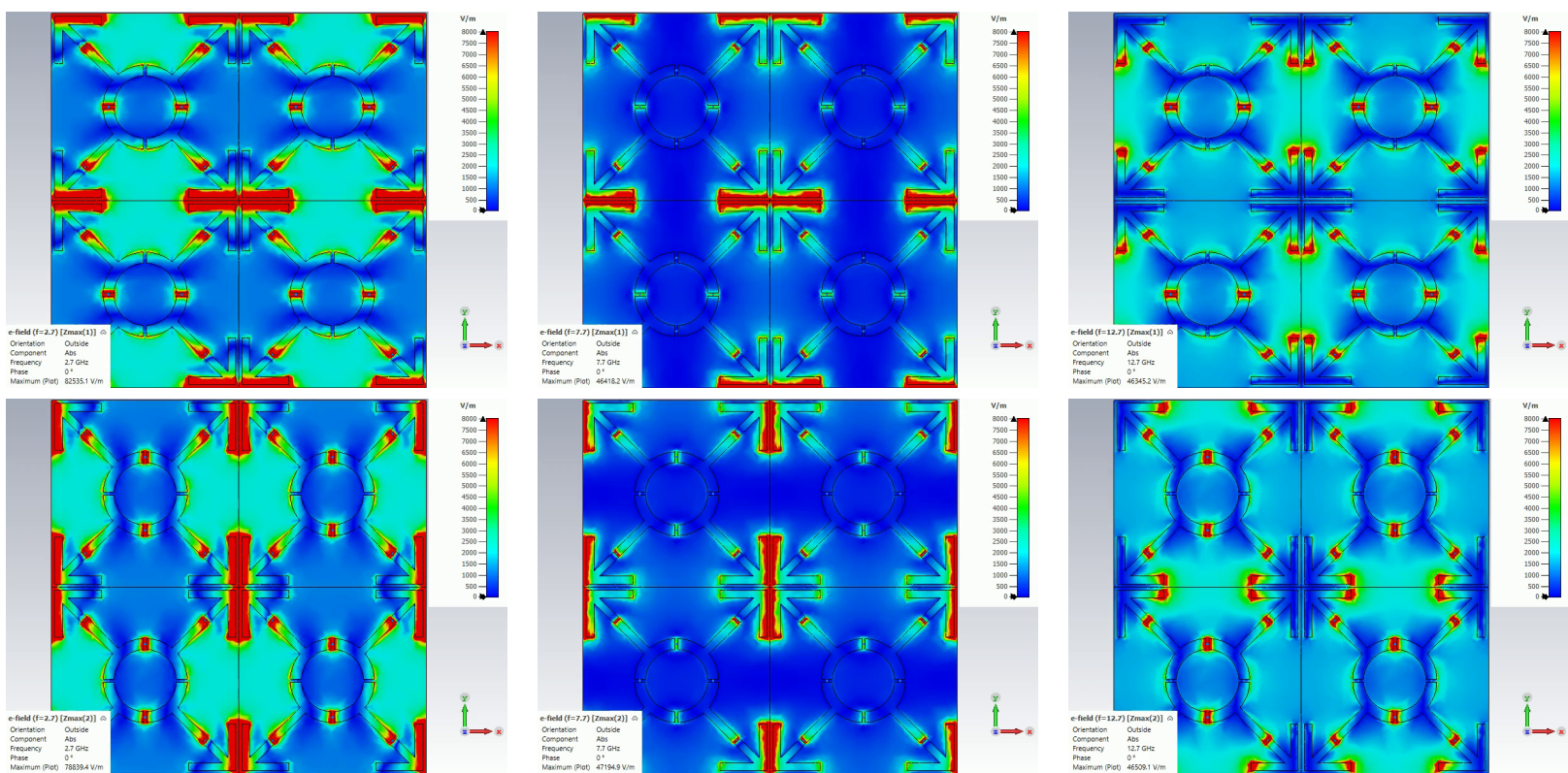
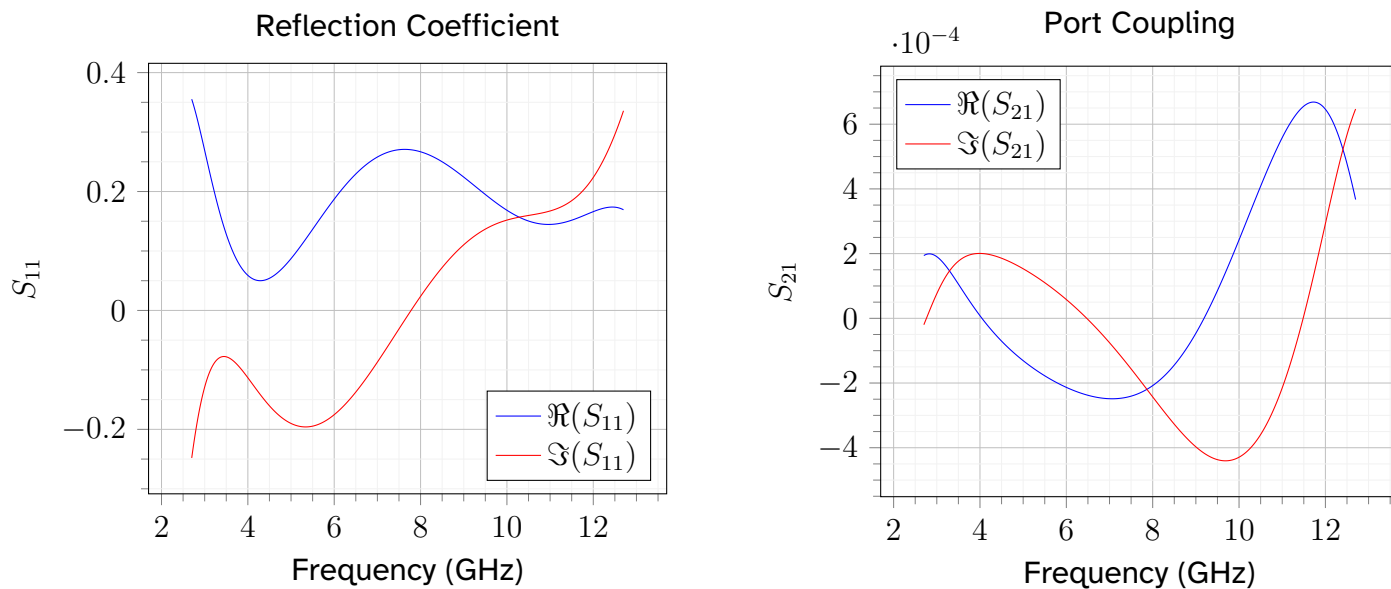
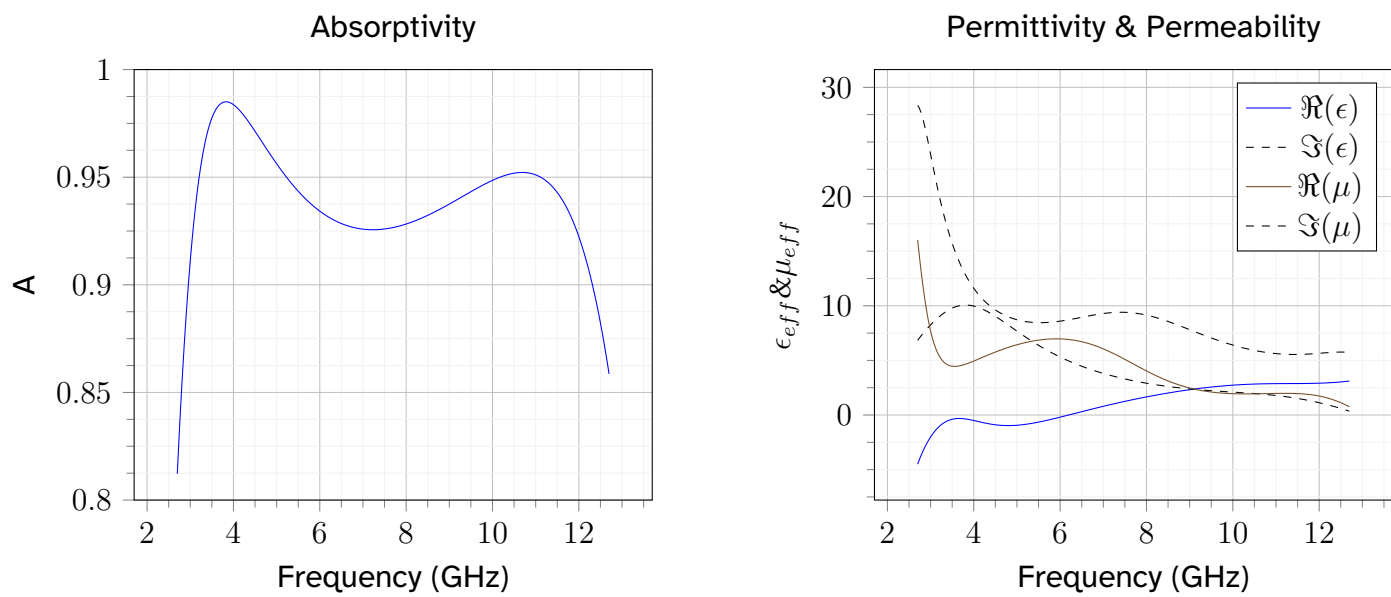


Figure 7: Electrical Field for [2.7, 7.7, 12.7] GHz Z_{max}

Taking a look in the S_{11} of Z_{max} that represents the reflection coefficient as well as the S_{21} that represents the port coupling, after the simulation as such (III.II). The Absorptivity (against the frequency) is an essential metric and CST calculates it as shown in (III.II). For the evaluation of the absorber Absorptivity can be calculated using the Fresnel equation: $A = 1 - R - T$, where T is the transmission coefficient (III.II) and can be calculated using the Fresnel equation: $T = \frac{2Z_0}{Z+Z_0}$ and R is the reflection coefficient (Γ) and can be calculated from the formula: $R = \frac{Z-Z_0}{Z+Z_0}$. However the Z mentioned needs to be the normalized impedance of the absorber so this is where the calculation will start.



The effective permittivity (ϵ) and permeability (μ) can be extracted from the S parameters but here are presented as extracted from the simulation in III.II.



III.III Alternative Modeling Methods

In addition to the CST simulation, there are several alternative methods to model the absorber:

- **Transmission Line Equivalent:** This method models the absorber as a transmission line, which can be useful for understanding the impedance matching and wave propagation.
- **Electrical Circuit Equivalent:** The absorber can be represented as an equivalent electrical circuit, simplifying the analysis of its behavior.
- **Mathematical Modeling & Code (MATLAB):** Numerical methods and coding in MATLAB can be used to simulate the absorber's performance, providing flexibility in parameter adjustments.

After completing the CST simulation, the impedance of the absorber can be extracted, which is useful for implementing the transmission line equivalent (8) model. For this the Z_{patch} is extracted from CST as the behavior of the absorber is related to the quality of impedance matching of the metal resonance layer which is connected in parallel to the impedances of the FR-4 substrate and the air layer respectively. Finally the copper backplate is represented as a sort circuit.

So the entire absorber can be modeled as a simple impedance matching problem with the basic equations in (1). The objective is for the equivalent impedance of the absorber to match the free space impedance and in order to simulate that with a transmission line equivalent the input impedances of each absorber layer shall be calculated. The input impedance of the air layer and the metal

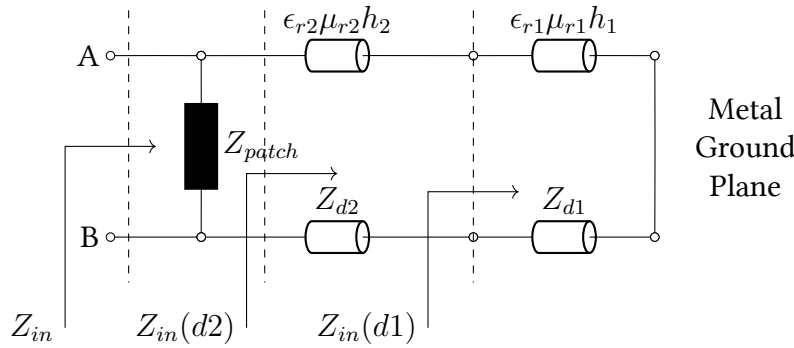


Figure 8: Transmission Line Equivalent

ground plane is calculated as in (3b) with the phase constant as in (3a). Then the FR-4 layer has a relative permittivity (ϵ) of 4.3 and a relative permeability (μ) of one but in the calculations the phase constant (3f) is derived from the loss tangent (3c) because the medium is way more dense than vacuum and thus the wavelength is less than $\frac{c_0}{f}$. So the input impedance of the combined FR-4, Air and Metal ground plane is calculated as in (3h).

$$\beta_1 = \frac{2\pi\sqrt{\mu_{r1}\epsilon_{r1}}}{\lambda} \quad (3a)$$

$$Z_{in}(d_1) = jZ_{d1} \tan \beta_1 h_1 = jZ_0 \sqrt{\frac{\mu_{r1}}{\epsilon_{r1}}} \tan \frac{2\pi h_1 \sqrt{\mu_{r1}\epsilon_{r1}}}{\lambda} \quad (3b)$$

$$\tan \delta = \frac{\sigma}{\omega \epsilon} = 0.025 \ll 1 \text{ where } \delta = \frac{1}{\alpha} \quad (3c)$$

$$\alpha = \frac{\sigma}{2} \sqrt{\frac{\mu_2}{\epsilon_2}} \Rightarrow \alpha = 40 \quad (3d)$$

$$\sigma = \sqrt{\frac{\epsilon_0 \epsilon_{r2} 2\alpha}{\mu_0 \mu_{r2}}} \quad (3e)$$

$$\beta_2 = \omega \sqrt{\frac{\mu_{r2} \mu_0 \epsilon_{r2} \epsilon_0}{2}} \left[\sqrt{1 + \left(\frac{\sigma}{\omega \epsilon_{r2} \epsilon_0} \right)^2} + 1 \right]^{\frac{1}{2}} \text{ where } \omega = 2\pi f \quad (3f)$$

$$Z_{d2} = Z_0 \sqrt{\frac{\mu_{r2}}{\epsilon_{r2}}} \quad (3g)$$

$$Z_{in}(d2) = Z_{d2} \frac{Z_{in}(d_1) + jZ_{d2} \tan \beta_2 h_2}{Z_{d2} + jZ_{in}(d_1) \tan \beta_2 h_2} \quad (3h)$$

The Z_{patch} is the impedance of the metal resonance layer and is extracted from the S parameters of the simulation. In greater detail the normalized impedance (or the intrinsic impedance) z for the entire absorber is expressed as (4a). And the refractive index can be expressed as (4b) using the S parameters.

$$z = \sqrt{\frac{(1 + S_{11})^2 - S_{21}^2}{(1 - S_{11})^2 + S_{21}^2}} \quad (4a)$$

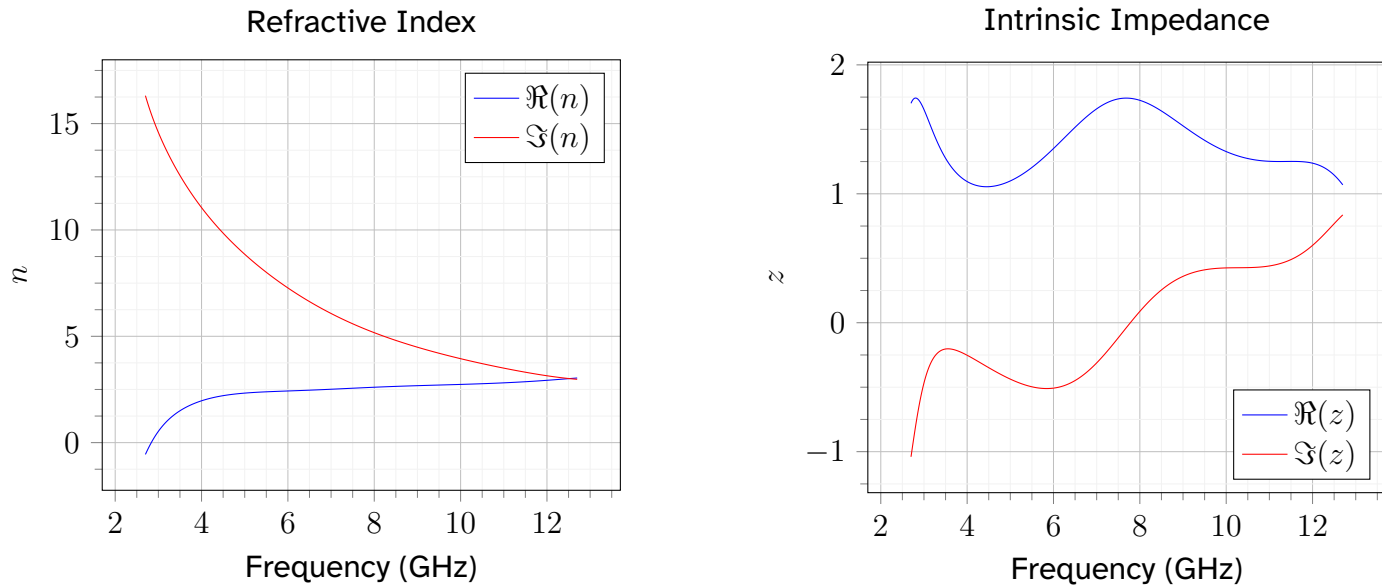
$$n = \frac{1}{kd} \arccos \left[\frac{1}{2S_{21}} (1 - S_{11}^2 + S_{21}^2) \right] \quad (4b)$$

The normalized impedance z is calculated as (III.III) and after it is multiplied with the free space impedance it gets denormalized $Z_L = z * Z_0$ so that the Z_{patch} can be extracted from (5a) and (5b).

$$\Gamma = \frac{Z_{patch} || Z_{in}(d_2) - Z_0}{Z_{patch} || Z_{in}(d_2) + Z_0} \quad (5a)$$

$$Z_L = \frac{1 + \Gamma}{1 - \Gamma} \quad (5b)$$

In the (III.III) and (III.III) however, the normalized ¹ impedance is calculated from CST after the simulation.



The exponential term that represents the phase of the wave across the entire frequency range. The wave number β is the same as κ in 4b.

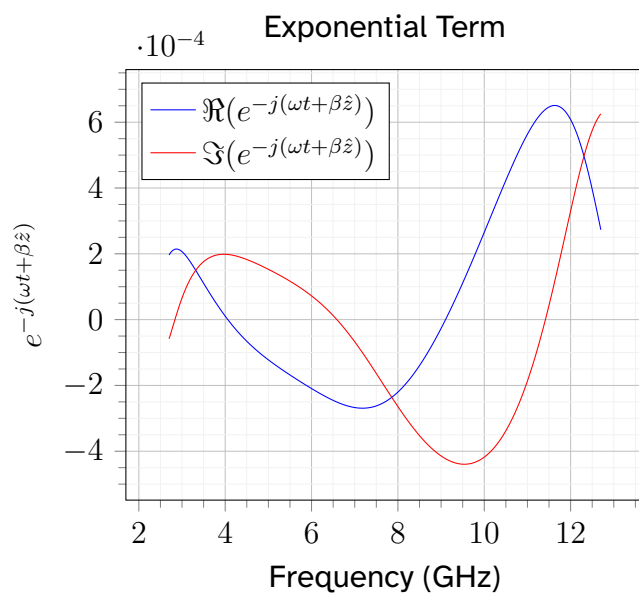


Figure 9: Exponential term against frequency

It is also worth noting that the absorber can be modeled as an equivalent electrical circuit (10). The difference with the transmission line equivalent (8) is that the absorber is in series between the free space impedance Z_0 and is modeled as two impedances of the FR-4 & Air layers in parallel to the impedance of the metal resonance layer.

This way the entire impedance characteristics of the absorber are the same with the transmission line equivalent (8) as they both match the free space.

¹or intrinsic

Figure 10: Electrical Circuit Equivalent

IV Optimization

In this modeling of the absorber the optimization is already done from the reference study [6]. However it is also possible to optimize the electrical circuit equivalent using the solvers provided in MATLAB. A method for the development of a circuit equivalent can be found in [3] and the relationship between physical dimensions and the material properties, and the electrical circuit components (e.g., the size of the metallic patterns, the thickness and permittivity of the dielectric layers). In greater detail, to define the optimization problem some properties of the absorber can be optimized to better maximize the absorbance and to do that the objective function is the absorbance itself as in (1d) but can also be extracted using the S parameters as in (6). Any constraints on the overall size and spacing will emerge from the optimization.

$$A(\omega) = 1 - |S_{11}(\omega)|^2 - |S_{21}(\omega)|^2 = 1 - R - T \quad (6)$$

To implement the optimization step using MATLAB two solvers can be invoked.

- `fmincon` : For constrained nonlinear optimization
- `ga` : For genetic algorithm-based optimization, which can be useful for complex problems with many local optima

For this study the `fmincon` shall be chosen and configured with the appropriate options:

- Initial State for the design variables
- Tolerance for convergence
- Maximum number of iterations

IV.I CST Optimizer

In this study however the optimization step will be performed by the built in optimizer in CST. In greater detail the parametric optimizer is used as it can optimize multiple parameters at once.

The parameters chosen to be optimized affect the resistor placement and the area around them as shown in figure (6a), these are:

- Lh : The height of resistor placement along the z axis with values between 0 and $d = 0.035mm$.
- Oa : The separation width near the arrows along the $y = x$ line with values between $0.001mm$ and $\sqrt{2}mm$.
- Oo : The separation with near the ring along the circle that has a radius of $r = r_1 + \frac{(r_2-r_1)}{2}$, with $r_1 = 2mm$ and $r_2 = 2.7mm$ and with values between $0.001mm$ and $0.1mm$ on each side $0.2mm$ in total.

After the simulation the Absorption is improved as well as the S parameters and the aforementioned variables end up with the following values:

- $Lh = 33.0166 \times 10^3mm$.
- $Oa = 49.8393 \times 10^3mm$.
- $Oo = 4.19669 \times 10^3mm$.

The optimized S parameters are mentioned in the table of figures (1) and in the S_{11} , the S_{21} and the exponential term the differences are visibly observable ². The Absorbance however, even though it appears to have increased on average across the frequency range, the difference is negligible.

CST provides a number of different solvers that can set Absorbance maximization as a goal function. For this optimization problem the Trust Region Framework is used. It is a local optimization solver that can be used globally doing multiple local optimizations for all parameters.

Initial goal function value = 0.0882249 (Solver)

Best goal function value = 0.0795194 (Solver)

Last goal function value = 0.0795194 (Solver)

Total solver time = 02:40:38 h (14 solver runs)

Total data recovery time = 00:00:31 h (2 loaded)

Total parameter update time = 00:02:33 h

Total backup project time = 00:00:45 h (4 backups)

Total optimizer time = 02:44:31 h (16 evaluations)

Optimization successfully improved the goal value. Best parameter set is stored.

It can be observed that the optimizer run 14 times which is considered small for three parameters and it is therefore possible to have hit a local minimum.

²The refractive index plot has been omitted as the optimization could not have affected it.

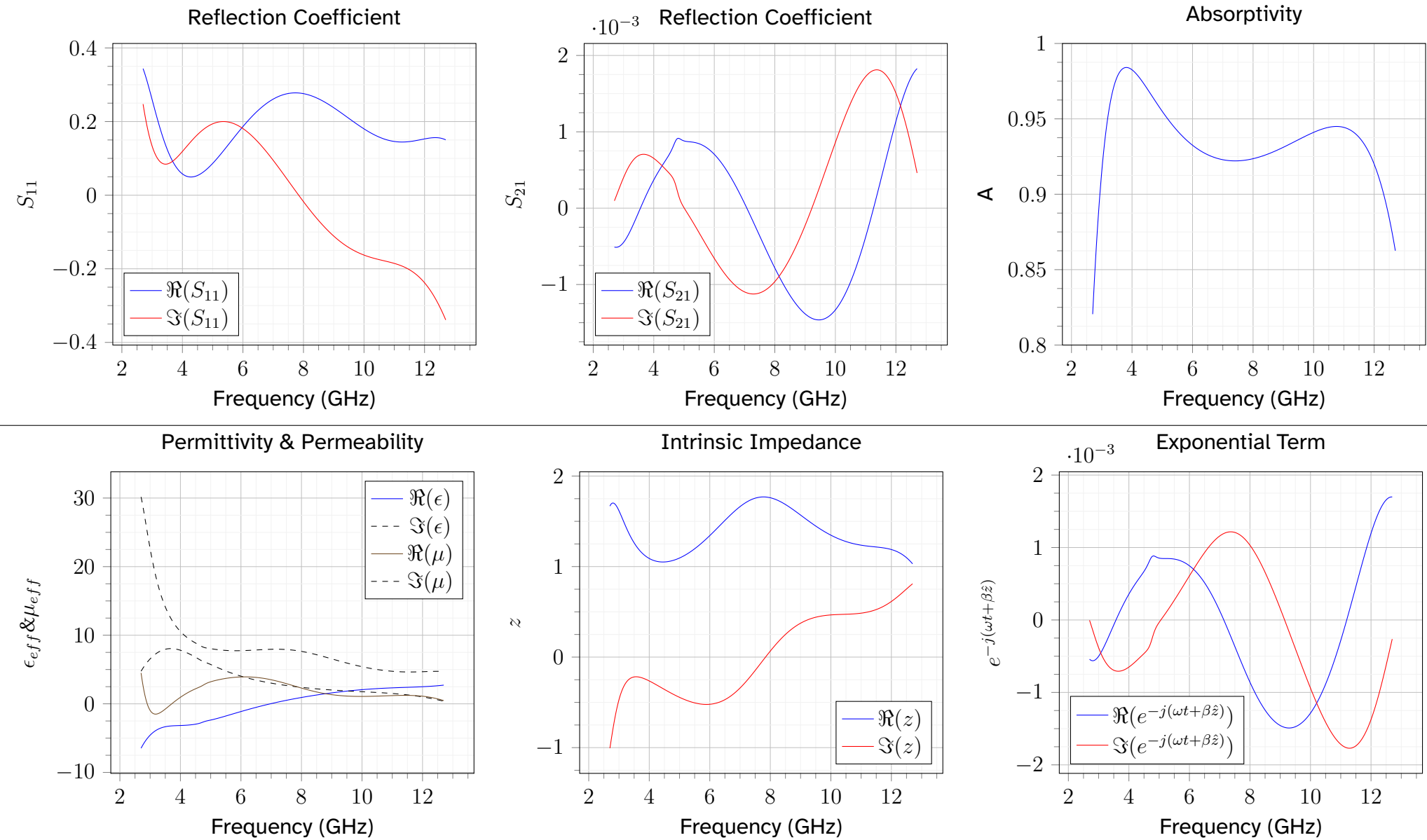


Table 1: Absorber Performance Indicators After the Optimization.

It is also worth stating that there are parameters that cannot be optimized using the method above. While equivalent circuit and transmission line models are valuable tools, they simplify the complex electromagnetic behavior of metamaterial absorbers.

- **Fine Geometric Details** : Equivalent circuit models often represent the metamaterial structure with lumped elements. Fine geometric details of the structure (e.g., the exact shape of the metallic patterns, small variations in dimensions) that can significantly affect the absorber's performance are not easily captured by these models.
- **Complex Electromagnetic Interactions** : Metamaterials exhibit complex electromagnetic interactions, such as near-field coupling between adjacent elements and high-order resonances. These effects may not be fully accounted for in simplified circuit models.
- **Angle of Incidence Effects** : The angle at which the electromagnetic wave hits the absorber can significantly affect its performance. Circuit models typically do not incorporate these angle-dependent effects accurately.
- **Polarization Effects** : While some circuit models can be adapted to consider polarization, accurately capturing complex polarization behavior, especially in anisotropic structures, can be challenging.
- **Material Dispersion** : The frequency dependence of the material properties (permittivity and permeability) can be difficult to model precisely with lumped circuit elements, especially over broad frequency ranges.

V Discussion

This study has demonstrated the potential of metamaterial-based microwave absorbers for achieving efficient electromagnetic wave absorption. The design and simulation of a specific absorber device, inspired by the structure presented [6], highlighted the key factors influencing its performance.

The results of the simulation showcase the ability of the metamaterial absorber to achieve high absorptivity across a broad range of frequencies. This is attributed to the unique electromagnetic properties of metamaterials, which allow for tailoring the absorption characteristics through precise structural design. The multi-layered structure of the absorber facilitates broadband absorption by creating multiple resonant frequencies.

However, it is important to acknowledge the trade-offs associated with optimizing the absorber's performance. For instance, while increasing the connection height between the copper faces near the arrows might enhance absorbance, it could also introduce additional complexities in the fabrication process. Similarly, achieving a perfect impedance match between the absorber and free space is crucial for minimizing reflection and maximizing absorption, but this can be challenging to achieve in practice due to various factors such as material losses and fabrication tolerances.

In terms of future improvements, there are several avenues to explore. One potential direction is to investigate different metamaterial structures and configurations to further enhance the absorber's bandwidth and absorption efficiency. For example, incorporating additional layers or varying the geometry of the metallic patterns could lead to improved performance.

Another area of focus could be on reducing the plasma frequency of metals in metamaterials. This would allow the absorbers to operate effectively at even lower frequencies, expanding their applicability to a wider range of electromagnetic environments. This can be achieved by manipulating the density of free electron carriers in the metal.

Furthermore, exploring alternative modeling methods, such as the transmission line equivalent and the electrical circuit equivalent, can provide additional insights into the absorber's behavior and aid in the optimization process. These methods offer different perspectives on the absorber's performance and can be used to validate the simulation results obtained from CST.

In conclusion, this study has provided a comprehensive analysis of a metamaterial-based microwave absorber, highlighting its potential for efficient EMI mitigation. While there are trade-offs to consider and challenges to overcome, the future of metamaterial

absorbers is promising. By continuing to explore new designs, materials, and modeling techniques, it is possible to further enhance their performance and expand their applications in various fields.

References

- [1] V. G. Veselago and E. E. Narimanov, "The left hand of brightness: Past, present and future of negative index materials," *Nature Materials*, vol. 5, no. 10, pp. 759–762, Oct. 1, 2006, ISSN: 1476-1122, 1476-4660. doi: 10.1038/nmat1746. [Online]. Available: <https://www.nature.com/articles/nmat1746> (visited on 11/05/2024).
- [2] Y. Wang, C. Lv, X. Zhang, X. Liu, and C. Zhang, "Simulation-guided design of gradient multilayer microwave absorber with tailored absorption performance," *Macromolecular Materials and Engineering*, vol. 309, no. 9, p. 2 400 015, Sep. 2024, ISSN: 1438-7492, 1439-2054. doi: 10.1002/mame.202400015. [Online]. Available: <https://onlinelibrary.wiley.com/doi/10.1002/mame.202400015> (visited on 11/05/2024).
- [3] K. R. Jha, G. Mishra, and S. K. Sharma, "Design of a compact microwave absorber using parameter retrieval method for wireless communication applications," *IET Microwaves, Antennas & Propagation*, vol. 12, no. 6, pp. 977–985, May 2018, ISSN: 1751-8733, 1751-8733. doi: 10.1049/iet-map.2017.0785. [Online]. Available: <https://onlinelibrary.wiley.com/doi/10.1049/iet-map.2017.0785> (visited on 11/05/2024).
- [4] M. C. Tran, V. H. Pham, T. H. Ho, *et al.*, "Broadband microwave coding metamaterial absorbers," *Scientific Reports*, vol. 10, no. 1, p. 1810, Feb. 4, 2020, ISSN: 2045-2322. doi: 10.1038/s41598-020-58774-1. [Online]. Available: <https://www.nature.com/articles/s41598-020-58774-1> (visited on 11/05/2024).
- [5] A. Biswas, C. L. Zekios, C. Ynchausti, L. L. Howell, S. P. Magleby, and S. V. Georgakopoulos, "An ultra-wideband origami microwave absorber," *Scientific Reports*, vol. 12, no. 1, p. 13 449, Aug. 4, 2022, ISSN: 2045-2322. doi: 10.1038/s41598-022-17648-4. [Online]. Available: <https://www.nature.com/articles/s41598-022-17648-4> (visited on 10/03/2024).
- [6] Y. Zhang, W. Yang, X. Li, and G. Liu, "Design and analysis of a broadband microwave metamaterial absorber," *IEEE Photonics Journal*, vol. 15, no. 3, pp. 1–10, Jun. 2023, ISSN: 1943-0655, 1943-0647. doi: 10.1109/JPHOT.2023.3277449. [Online]. Available: <https://ieeexplore.ieee.org/document/10129034/> (visited on 11/05/2024).